Catalysis Science & Technology

ROYAL SOCIETY OF CHEMISTRY

PAPER

View Article Online
View Journal | View Issue

Cite this: *Catal. Sci. Technol.*, 2020, **10**, 5935

Gold–palladium colloids as catalysts for hydrogen peroxide synthesis, degradation and methane oxidation: effect of the PVP stabiliser†

Simon J. Freakley, *[a] Nishtha Agarwal,[b] Rebecca U. McVicker,[b] Sultan Althahban,[cd] Richard J. Lewis, [b] David J. Morgan, [b] Nikolaos Dimitratos,[e] Christopher J. Kiely[bc] and Graham J. Hutchings *[b]

The reactivity of AuPd nanoparticle catalysts prepared by sol immobilisation is often explained by a structure activity relationship based solely on particle size or composition. In this contribution, we compare colloidal AuPd nanoparticles stabilised with polyvinylpyrrolidone (PVP) with the same AuPd nanoparticles supported on TiO_2 for the direct synthesis of hydrogen peroxide and methane oxidation to methanol. We show that while the particles have similar rates of H_2O_2 synthesis, supporting the particles can affect the rates of H_2O_2 decomposition and hence the effectiveness of the catalyst for reactions which rely on H_2O_2 as an initiator or oxidant. We demonstrate that the absence of PVP results in high rates of H_2O_2 decomposition in methane oxidation experiments but this can be minimised by the addition of PVP to the reactor. These results also show that for AuPd alloys, both polymer stabiliser and support effects need to be taken into account when describing the activity of the nanoparticles and the active sites should in fact be thought of as a metal–support–polymer interface with many degrees of freedom.

Received 5th May 2020,
Accepted 6th August 2020

DOI: 10.1039/d0cy00915f

rsc.li/catalysis

Introduction

The preparation of supported precious metal catalysts by colloidal nanoparticle synthesis methods can result in highly active materials for a range of important chemical processes.[1,2] The advantage of solution phase synthesis of metal nanoparticles is the high degree of control over the particle size, shape and composition that can be achieved before immobilisation onto high surface area supports.[3] Typically, colloidal methods involve fast chemical reduction of metal precursors and steric stabilisation of the growing nanoparticles by polymer additives.[4] In many cases these catalysts are used without high temperature oxidative heat treatments or washing protocols specifically designed to remove the strongly bound polymer.[5–7] Therefore, in reality the reported performance of the catalyst material not only depends on the nature of the metal particle (size, shape, oxidation state) but also the nature of the composite particle–polymer surface.

Reaction rates, product selectivity and enantioselectivity can all be altered by the interaction of the polymer ligand or organic modifier with the metal surface.[8] For instance, the introduction of chiral modifiers such as cinchonidine derivatives or napthyl-ethylamine to Pt catalysts have been shown to impart increased enantioselectivity in activated ketone hydrogenation.[9–11] Polymer additives can also be used to tune the oxidation states of metal surfaces through binding of electron donating or withdrawing groups which in turn effects reactant binding strengths.[12] Steric effects can also be observed in many cases with changes in reaction selectivity observed in the presence of polymer additives.[13] Despite these potential advantageous degrees of control available by polymer addition, detrimental effects such as site blocking by strong adsorption can reduce activity – especially in gas phase reactions.[14–16] This requires careful removal of polymer additives prior to reaction without significantly changing the nanostructure of the catalyst material which has been carefully controlled in the colloidal synthesis of the nanoparticles.

Polyvinylpyrrolidone (PVP) is a common polymer additive used in the preparation of precious metal catalysts for

[a] *Department of Chemistry, University of Bath, Claverton Down, Bath, BA2 7AY, UK. E-mail: s.freakley@bath.ac.uk*
[b] *Cardiff Catalysis Institute and School of Chemistry, Main Building, Park Place, Cardiff, CF10 3AT, UK. E-mail: hutch@cardiff.ac.uk*
[c] *Department of Materials Science and Engineering, Lehigh University, 5 East Packer Avenue, Bethlehem, PA 18015, USA*
[d] *Department of Mechanical Engineering, Jazan University, Jazan 82822, Saudi Arabia*
[e] *Department of Industrial Chemistry, Alma Mater Studiorum-University of Bologna, Viale Risorgimento, 40136, Bologna, Italy*

† Electronic supplementary information (ESI) available. See DOI: 10.1039/d0cy00915f

reactions such as glycerol oxidation using Au and Pd based catalysts supported on TiO_2.[17–20] We recently demonstrated that while effective catalysts could be prepared in the absence of additives, the presence of PVP and polyvinylalcohol (PVA) has significant effects on product selectivity which is often not considered in structure activity relationships.[21,22] Similar catalyst structures based on Au–Pd particles have been shown to be highly active for reactions such as the direct synthesis of hydrogen peroxide (H_2O_2) from molecular hydrogen and oxygen which would represent an attractive alternative to the current indirect anthraquinone process for on-site H_2O_2 production.[23–27] Catalysts with varying alloy compositions and nanostructure have been extensively studied for this reaction and have been shown to be highly active for H_2O_2 synthesis.[27] Titania supported Au–Pd catalysts prepared by colloidal methods with small particle sizes tend to have significant activity for H_2O_2 degradation by over hydrogenation and decomposition.[28] To date, the challenge of minimising the subsequent degradation of H_2O_2 (*via* hydrogenation and decomposition pathways) has only been achieved with a few specific catalyst systems in the absence of acid and halide additives.[29–31]

Unsupported colloidal nanoparticles can be active for a number of reactions including glucose oxidation,[32] aromatic alcohol oxidation[33] and CO_2 reduction.[34] Nomura *et al.* have previously reported that unsupported AuPd colloidal particles can be active for the direct synthesis of H_2O_2 from H_2 and O_2.[35] Recent studies by Deguchi *et al.* have shown that a range of bimetallic colloidal particles stabilised with PVP, including Pd–Ir and Pd–Pt, can be active catalysts – however the role of the polymer additive in all these cases has not been explicitly addressed.[36] Recently we demonstrated that using colloidal AuPd nanoparticles stabilised with PVP, it was possible to achieve selective oxidation of methane to methanol at 25–50 °C with O_2 incorporation using H_2O_2 as an initiator.[37] A significant result in this study showed that the background H_2O_2 decomposition rate was minimal for unsupported colloidal AuPd–PVP particles at 50 °C, allowing the radical reaction process to propagate rather than terminate; however the H_2O_2 decomposition rate increased significantly when then the same particles were supported on TiO_2 making this an ineffective catalyst.[37]

This result clearly demonstrated that colloidal particles stabilised by polymers can have significantly different behaviour in reactions involving H_2O_2 than analogous 'bare' particles supported on TiO_2 and while colloidal catalyst systems could have limitations in terms of long term stability it is possible to use them to propose structure–activity relations. In this study, we aim to elucidate if the PVP stabilisers present on AuPd particles effect the H_2O_2 synthesis and methane oxidation reaction networks and investigate if the reactivity in these systems should be considered as not only a result of interactions with the surface atoms on the metal nanoparticle, but rather with an entity more akin to a metal core–polymer shell composite.

Results and discussion

Recent studies by Giorgianni *et al.* reported that the addition of PVA to Pd catalysts results in enhanced H_2O_2 yields due to hindered H_2O_2 back diffusion to the metal surface *via* hydrophobic interactions in addition to greater observed catalyst stability when PVA is present.[38] In this current study on H_2O_2 synthesis and methane oxidation, we focus on PVP as an additive because in methane oxidation reactions traces of MeOH have been previously observed as a result of PVA contamination or oxidative degradation under our reaction conditions. A series Au–Pd colloidal nanoparticle solutions were synthesised according to previously described procedures.[37] The colloidal solutions of Au–Pd nanoparticles (Au : Pd = 1 : 1 by moles) were synthesised *via* $NaBH_4$ reduction of metal salts and stabilised by PVP. A portion of the AuPd–PVP colloidal nanoparticles were immobilised onto TiO_2 (1 wt% metal loading) and dried at 110 °C to provide comparative supported samples. Both the supported and unsupported AuPd–PVP materials were then tested for the direct synthesis of H_2O_2 and methane oxidation, using experimental conditions which have both been previously described in the literature.[28,37]

The colloidal metal nanoparticles and the supported colloidal nanoparticles have been previously characterised by X-ray photoelectron spectroscopy.[37] XPS analysis of the colloidal AuPd–PVP nanoparticle solution in the Au(4f) and Pd(3d)/Au(4d) regions, after drop casting onto a solvent cleaned silicon wafer, showed that both elements were present in predominantly the metallic state (Au(4f) ~ 83–84 eV, Pd(3d) ~ 334.5–335.5 eV, the range in energies varying depending on particle size and support interactions) as could be expected from the presence of the strong reducing agent at the high molar ratio used in the preparation. For the unsupported colloid, a Au signal at 85.5 eV and a Pd signal (*ca.* 388 eV) were also detected and attributed to residual or leached metal chlorides. XPS analysis of the immobilised nanoparticles exhibit both Au and Pd binding energies *ca.* 1 eV lower compared to the unsupported colloid. Such low Pd binding energies may be attributed to a particle–support interaction making the zero-valent supported Pd more electron rich. The corresponding Au($4f_{7/2}$) signal exhibits a binding energy of 83.1 eV and lower than the characteristic 84 eV for bulk Au, although such binding energies have been widely reported, and are typically attributed to small, low coordination atoms, charge transfer from PVP to Au, and charge transfer between Pd and Au, increasing the s-state occupancy of Au indicating alloy formation.[39,40]

TEM analysis (Fig. 1a and b) showed that the mean size of the bimetallic particles in the colloidal solution was 3.0 ± 2.0 nm, which increased slightly to 4.1 ± 1.3 nm when the particles were immobilised onto the support. This is in good agreement with our previous studies on these materials where the apparent increase in size occurs as a result of the AuPd nanoparticle flattening slightly and faceting to form an interface with the TiO_2 support (Fig. 1c and d).[28]

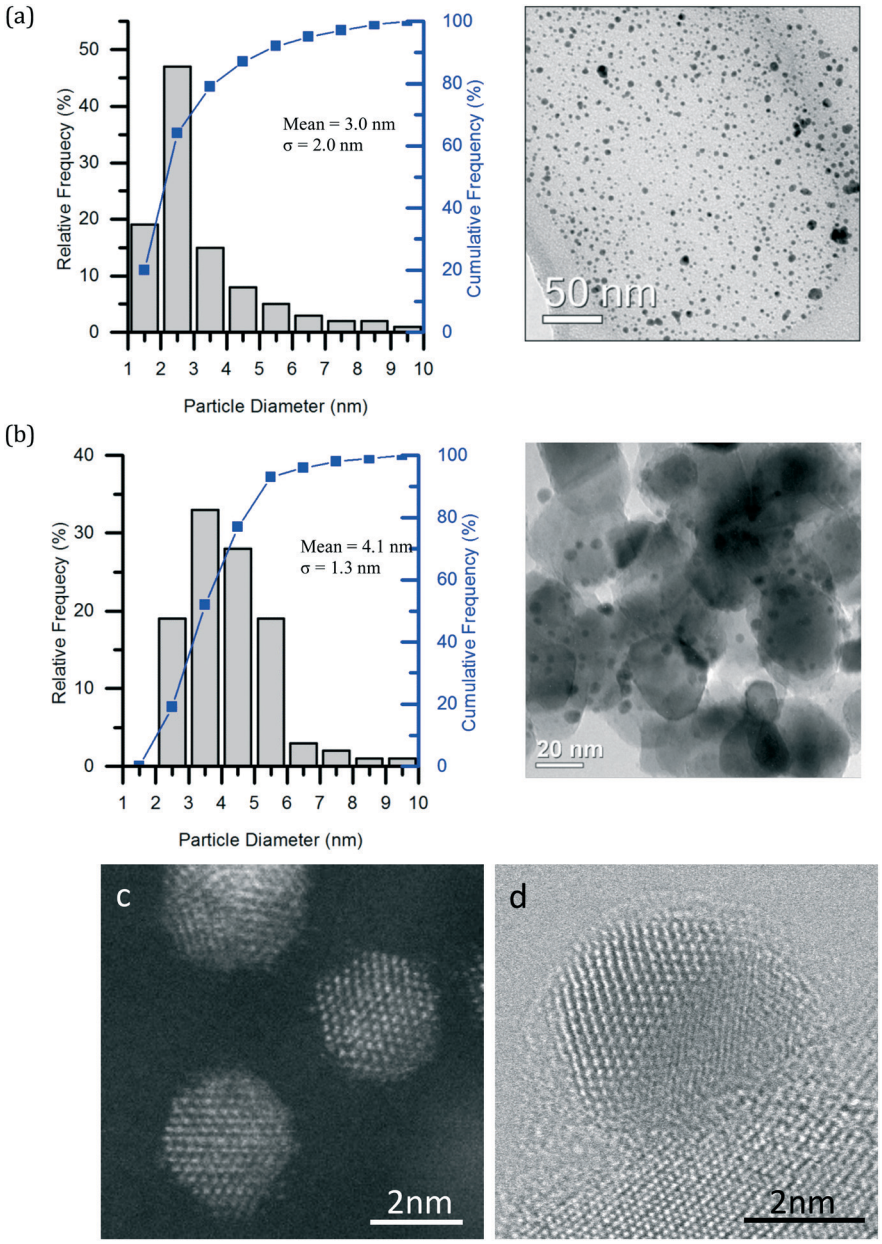

Fig. 1 BF-TEM images and corresponding particle size distributions of (a) colloidal and (b) TiO_2 supported Au–Pd nanoparticles prepared by sol-immobilisation using PVP as the stabiliser. (c) HAADF image of Au–Pd–PVP colloidal particles drop cast onto a C TEM gird. (d) HR-TEM phase contrast lattice image of a typical AuPd–PVP particle supported on TiO_2.

Previous studies have demonstrated that colloidal Pd and AuPd–PVP nanoparticles, in the presence of strong acid and halide additives, can produce H_2O_2 *via* the direct reaction of H_2 and O_2.[41] These un-supported particles were stabilised by PVP and were shown to exhibit appreciable rates for direct H_2O_2 synthesis suggesting that the presence of a support is not essential for high activity in this reaction. We carried out comparative tests between our colloidal AuPd–PVP materials in the unsupported and TiO_2 supported state ensuring that each reaction had the equivalent moles of metal (0.66 μmol). The results, shown in Table 1, entries 1–3, demonstrate that over a 30 min reaction period the unsupported colloidal Au–Pd–PVP nanoparticles were capable of producing 0.10 wt% H_2O_2 compared to 0.07 wt% H_2O_2 when using TiO_2 supported counterparts; their corresponding apparent turnover frequencies (TOFs) based on total moles of metal were 8.0×10^2 and 5.2×10^2 $mol_{H_2O_2}$ mol_{metal}^{-1} h^1 respectively. The TiO_2 support alone showed no background activity towards H_2O_2 synthesis or H_2O_2 degradation (*via* over-hydrogenation or decomposition). Next, the amount of AuPd–PVP colloidal nanoparticle solution used was varied to identify the kinetic regime in which the reaction was operating. Fig. 2 shows that increasing the amount of Au–Pd colloidal nanoparticle solution added to the reaction results

Table 1 Summary of catalytic testing results for the various AuPd–PVP catalyst systems tested for H_2O_2 synthesis, degradation and decomposition

Entry	Catalyst	PVP: M	H_2O_2[a] (wt%)	Apparent reaction rate at 30 min ($mol_{H_2O_2}$ mol_{metal}^{-1} h^{-1})	Apparent reaction rate at 30 min ($mol_{H_2O_2}$ $mol_{surface}^{-1}$ h^{-1})[d]	H_2O_2 degradation[b] (%)	H_2O_2 decomp.[c] (%)
1	AuPd colloid	1.2	0.10	8.0×10^2	2.7×10^4	13	1
2	1% AuPd/TiO_2	1.2	0.07	5.2×10^2	3.2×10^4	11	7
3	TiO_2	0	0.00	—	—	0	0
4	1% AuPd/C	1.2	0.13	10×10^3	—	9	1
5	AuPd colloid	0.005	0.08	6.2×10^2	2.8×10^4	9	0
6	AuPd colloid	0.1	0.11	8.5×10^2	2.6×10^4	11	1
7	AuPd colloid	20	0.12	9.1×10^2	2.7×10^4	13	1
8	AuPd colloid	0	0.07	5.2×10^2	—	11	7

[a] H_2O_2 synthesis conditions: 5% H_2/CO_2 (29 bar) and 25% O_2/CO_2 (11 bar), 8.5 g solvent (2.9 g HPLC 5.6 g MeOH), 0.66 μmol metal, reaction temperature = 2 °C, stirring rate = 1200 rpm, reaction time = 30 min. [b] H_2O_2 degradation conditions: 5% H_2/CO_2 (29 bar), 8.5 g solvent (5.6 g MeOH, 2.22 g H_2O and 0.68 g 50% H_2O_2), 0.66 μmol metal, reaction temperature = 2 °C, stirring rate = 1200 rpm, reaction time = 30 min. [c] H_2O_2 decomposition conditions: 25% O_2/CO_2 (29 bar), 8.5 g solvent (5.6 g MeOH, 2.22 g H_2O and 0.68 g 50% H_2O_2), 0.66 μmol metal, reaction temperature = 2 °C, stirring rate = 1200 rpm, reaction time = 30 min. [d] As determined from measured TEM particle size distributions.

in a linear increase in the amount of H_2O_2 produced, reaching 0.29 wt% after 30 min reaction, which was the point where the 2.9 mL H_2O used as solvent was completely replaced by the aqueous AuPd–PVP colloidal solution. This result indicated that no external gas–liquid diffusion limitations were occurring when increasing amounts of the colloidal catalyst were used in the reaction. This finding is in contrast to our previous studies using TiO_2 supported AuPd catalysts where a plateau is observed in H_2O_2 yield with increasing catalyst mass due to mass transfer effects.[42]

Over a 30 min reaction time, significant H_2O_2 degradation is likely when using Pd containing nanoparticles in the 2–5 nm size range, with halide and acid stabilisers typically used to minimize degradation pathways, suggesting that the reported TOFs after 30 min of reaction are under-estimates of the actual TOFs, because some fraction of the H_2O_2 produced will have been destroyed by subsequent over-hydrogenation or decomposition reactions.[43] Fig. 3 shows a comparison in terms of wt% H_2O_2 produced of the colloidal metal nanoparticle solution and supported AuPd catalyst as a function of time for this reaction. It can be seen that at very short reaction times, (~2 min) where the contribution from H_2O_2 degradation pathways can be assumed to be negligible, that the colloidal AuPd–PVP nanoparticle solution has a higher initial rate of H_2O_2 synthesis than the corresponding supported AuPd nanoparticles. A turnover frequency of 4630 $mol_{H_2O_2}$ mol_{metal}^{-1} h^1 was determined for the unsupported colloid as compared to 2140 $mol_{H_2O_2}$ mol_{metal}^{-1} h^1 for the TiO_2 supported AuPd nanoparticles based on the total moles of metal present in this regime where subsequent reactions are minimised.

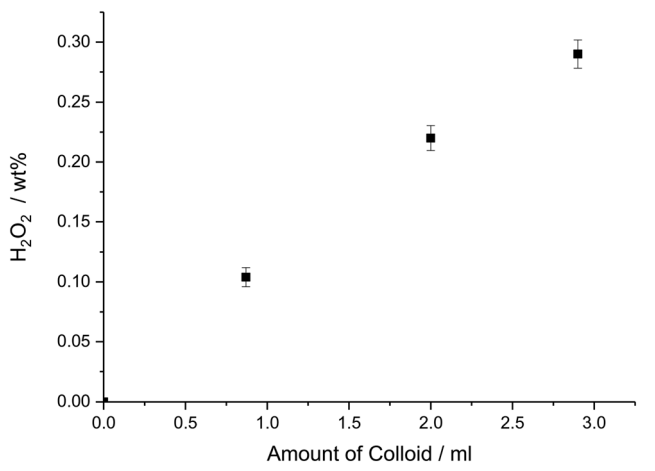

Fig. 2 H_2O_2 produced with increasing amounts of unsupported Au–Pd colloid added to the reaction solution up to complete replacement of the H_2O in the solvent system (2.9 ml). H_2O_2 synthesis conditions: 5% H_2/CO_2 (29 bar) and 25% O_2/CO_2 (11 bar), 8.5 g solvent (2.9 g HPLC 5.6 g MeOH), colloidal solution concentration [0.66 mM_{metal}], reaction temperature = 2 °C, stirring rate = 1200 rpm, reaction time = 30 min.

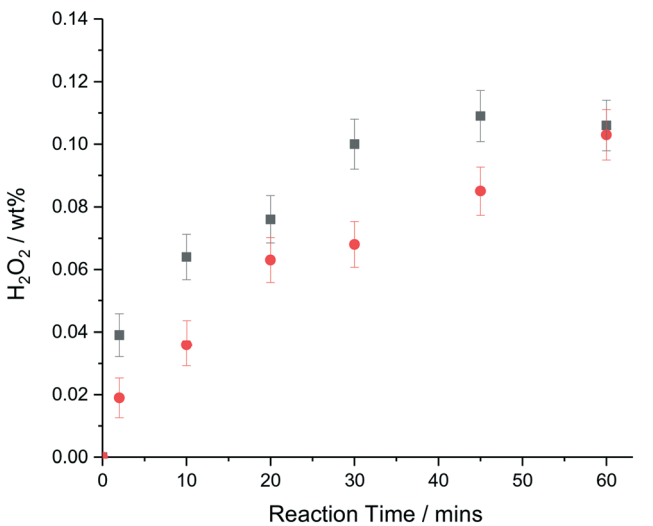

Fig. 3 H_2O_2 produced (wt%) as a function of reaction time by unsupported and TiO_2 supported AuPd–PVP colloid nanoparticles. wt% H_2O_2 produced – filled symbols; colloidal particles (■), supported particles (●). H_2O_2 synthesis conditions: 5% H_2/CO_2 (29 bar) and 25% O_2/CO_2 (11 bar), 8.5 g solvent (2.9 g HPLC 5.6 g MeOH), 0.66 μmol metal, reaction temperature = 2 °C, stirring rate = 1200 rpm;, reaction time = 30 min.

Due to the measured difference in particle size distribution of the two catalytic systems, the total number of surface atoms available in each reaction was estimated using the particle size distributions obtained by TEM and applying the same model for atom packing to each system. This approximation assumes activity is related to the total number of exposed surface atoms and is not correlated with specific surface sites such as edges or corner atoms. In addition it assumes that the polymer coverage of the metal surface is consistent between both samples. This analysis gave 1.2×10^{17} surface atoms for the colloidal system assuming spherical particles *versus* 5.7×10^{16} for the TiO_2 supported catalyst assuming hemispherical supported particles meaning that the colloidal samples have ~2.1 times the exposed metal surface. Based on the amount of H_2O_2 produced after 2 min of reaction, where the contribution from subsequent reactions (hydrogenation and decomposition) is minimal, we find that the moles of H_2O_2 produced at each exposed surface site is comparable between the colloidal metal nanoparticle solution (1.7×10^{-21} $mol_{H_2O_2}$ metal site^{-1} h^{-1}) and the supported AuPd nanoparticles (1.5×10^{-21} $mol_{H_2O_2}$ per metal site per h). Considering the assumptions made during this comparison this suggests that H_2O_2 formation occurs on the surface of the Au–Pd nanoparticles at similar rates in both catalytic systems when minimal H_2O_2 degradation pathways are operating. Due to the large difference in catalyst mass between colloidal and supported nanoparticle catalysts rates normalised to both total moles of metal and moles of metal surface for 30 min reactions are reported in Table 1 assuming no significant change in the catalyst structure takes place.

Experiments were also carried out to investigate the effect that supporting the colloidal AuPd–PVP nanoparticles on TiO_2 had on the degradation of a 4 wt% H_2O_2 solution, which included contributions from both H_2O_2 hydrogenation and decomposition pathways. Comparing the unsupported colloidal AuPd–PVP solution to the corresponding TiO_2 supported catalyst, the total degradation after 30 min (Table 1, entries 1–2) was similar for both situations. However, when normalising to the difference in surface sites between the colloidal and supported nanoparticles, it is clear to see that the supported particles have significant higher rates per metal surface site by a factor of ~2.5. By comparing the rates of H_2O_2 decomposition under a 25% O_2/CO_2 atmosphere to remove over-hydrogenation from the possible reaction pathways, it was observed that the colloidal AuPd–PVP solution decomposed only 1% of the H_2O_2 present compared to the supported particles which decomposed 7% of the initial H_2O_2 suggesting a significant difference in how the two samples interact with H_2O_2.

The decomposition of H_2O_2 occurs much faster when the Au–Pd particles are supported on TiO_2, despite the supported particles having larger mean particle size and therefore less exposed surface available (by roughly a factor of 2) meaning an increase in observed decomposition rate of about 14 times for the supported particles as compared to the unsupported colloidal particles. Assuming that the H_2O_2 hydrogenation and decomposition pathways are independent of each other, this suggests that either it is the act of supporting the particles which generates a metal–metal oxide support interface or the removal of PVP on washing the solid which changes the predominant H_2O_2 degradation pathway. Our previous studies have shown that supporting Au colloids on crystalline metal oxides such as TiO_2 results in a more highly faceted particle structure than when they are supported on amorphous carbon structures.[14,15,44] We prepared an analogous sample by supporting the same colloidal AuPd nanoparticle solution on an activated carbon. This sample showed higher H_2O_2 production, but also no H_2O_2 decomposition activity, supporting the notion that immobilisation of the AuPd colloid onto TiO_2 P25 surface results in increased H_2O_2 decomposition rates possibly through the formation of highly faceted surfaces as the particle restructures to minimise the energy needed to interact with the underlying support lattice and form an extended intimate support/metal interface. This highlights the possibility that the underlying support material can possibly indirectly effect the decomposition pathways of H_2O_2 on the surfaces of the alloy nanoparticle attached to it.

Numerous observations that supported catalysts prepared from PVP-stabilised colloids show low activity in gas phase reactions, such as CO oxidation, due to the presence of residual polymer suggest that the polymer is still present to some extent after the preparation of the supported catalyst material.[15,16] Further studies by Han *et al.* report the stability of the PVP polymer under H_2O_2 synthesis conditions similar to those used within this work supporting the hypothesis that PVP is stable to the reaction conditions used in this study.[6] To further investigate if the presence of PVP contributes to these effects colloidal Au–Pd nanoparticles were prepared using a variety of PVP : metal ratios between 20 and 0.005 in order to study the influence of PVP concentration and particle size on the reaction, (Table 1 entries 5–7, Fig. 4). The mean particle size of the colloidal particles ranged from 6 ± 1.9 nm for a PVP/metal ratio of 0.05 to 1.9 ± 1.3 nm for a PVP/metal ratio of 20. This decrease in mean size correlates well with the increasing amount of polymer allowing the formation of a higher number of smaller nuclei during the preparation. Fig. 4 shows that as the average particle size of the AuPd nanoparticles decreases, the net amount of H_2O_2 produced after 30 min of reaction increases from 0.08 wt% for 6 nm particles to 0.12 wt% for 1.9 nm particles. In all cases, the colloidal AuPd–PVP particles showed minimal H_2O_2 decomposition (Table 1, entry 5–7), even when the solution contained smaller particles (*i.e.,* a greater number of exposed metal surface atoms) producing higher amounts of H_2O_2 over the 30 min reaction. Fig. 4b reports the normalised rate per surface atom as approximated by the TEM derived particle size distributions for a range of catalysts prepared with various PVP to metal ratios for H_2O_2 synthesis, degradation and decomposition. No significant change in apparent TOF per surface atom was observed over the mean

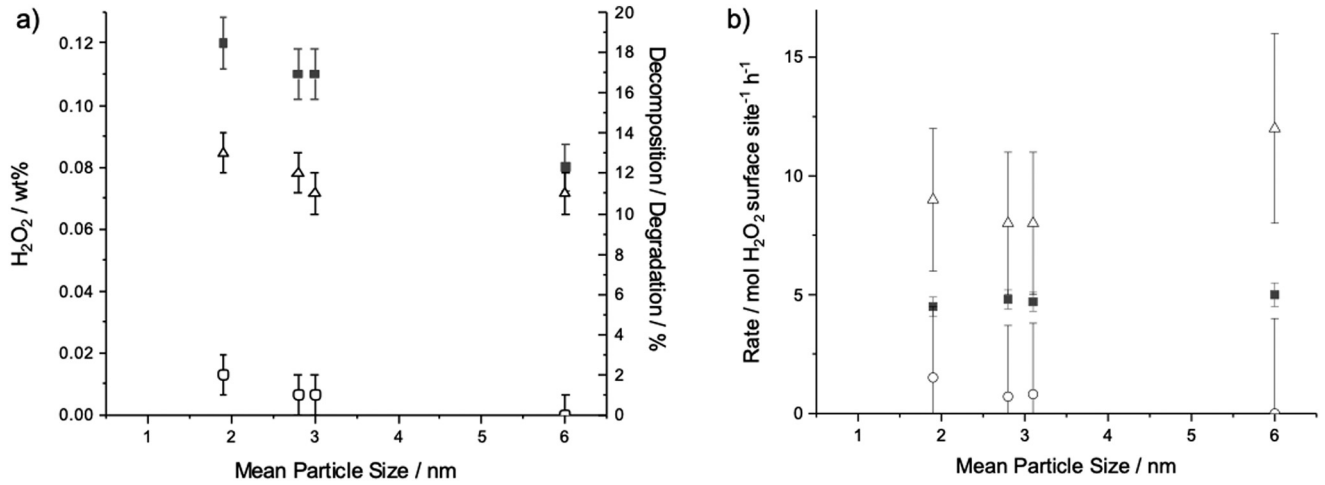

Fig. 4 a) Catalytic activity results for unsupported AuPd–PVP colloidal nanoparticle solutions prepared with various amounts of PVP giving rise to different mean nanoparticle sizes. b) Rate normalised to available metal surface as determined by TEM particle size distributions. Key to symbols; wt% H_2O_2 produced (■), H_2O_2 degradation (△) and H_2O_2 decomposition (○). H_2O_2 synthesis conditions: 5% H_2/CO_2 (29 bar) and 25% O_2/CO_2 (11 bar), 8.5 g solvent (2.9 g HPLC 5.6 g MeOH), 0.66 μmol metal, reaction temperature = 2 °C, stirring rate = 1200 rpm, reaction time = 30 min. H_2O_2 degradation conditions: 5% H_2/CO_2 (29 bar), 8.5 g solvent (5.6 g MeOH, 2.22 g H_2O and 0.68 g 50% H_2O_2), 0.66 μmol metal, reaction temperature = 2 °C, stirring rate = 1200 rpm, reaction time = 30 min. H_2O_2 decomposition conditions: 25% O_2/CO_2 (29 bar), 8.5 g solvent (5.6 g MeOH, 2.22 g H_2O and 0.68 g 50% H_2O_2), 0.66 μmol metal, reaction temperature = 2 °C, stirring rate = 1200 rpm, reaction time = 30 min.

particle size range 1.9 to 6.0 nm, however it should be noted that these reaction rates were determined after 30 min so do not represent initial rates which are independent of subsequent reaction processes. This suggests, due to the minimised H_2O_2 decomposition in all colloidal samples compared to the supported sample, that it is the effect of supporting the particles and their interaction with the TiO_2 lattice that initiates H_2O_2 decomposition in this system and that the main loss of H_2O_2 selectivity using colloidal particles results from over hydrogenation.

To support our conclusions, we investigated the decomposition of H_2O_2 by simply stirring both supported and unsupported catalytic systems in glass vials containing 4 wt% H_2O_2 under air at ambient conditions, rather than at 2 °C and under a 29 bar pressure of 5% H_2/CO_2 as in the regular H_2O_2 synthesis experiments. Fig. 5 shows that when TiO_2 and the AuPd–PVP sol were stirred separately with the starting H_2O_2 solution, approximately 4–5% of the H_2O_2 was decomposed over the 30 min reaction period. In contrast, when the supported 1wt% AuPd/TiO_2 material was tested, containing the same amount of metal, bubbles of gas generated from the decomposition of H_2O_2 were clearly visible originating from the catalyst. Over the same 30 min time period, approximately 80% of the H_2O_2 was decomposed. Furthermore, addition of varying extra amounts of PVP to the solution did not suppress the rapid gas generation.

Astruc and co-workers have demonstrated that it is possible to prepare colloidal Au catalysts in the absence of polymer stabilisers relying solely on electrostatic stabilisation of the metal particles by residual salts in the colloidal solution.[45] We recently showed that it is possible to prepare supported AuPd catalysts in a similar manner with a slightly broader particle size distribution compared to conventional immobilisation of polymer stabilised colloidal solutions.[22] This colloidal nanoparticle solution prepared without polymer addition (denoted SF-stabiliser free) was also tested for direct H_2O_2 synthesis (Table 1, entry 8). Interestingly they showed activity towards H_2O_2 production and also increased rates of H_2O_2 decomposition suggesting that the greater accessibility to the surface in the absence of PVP results in

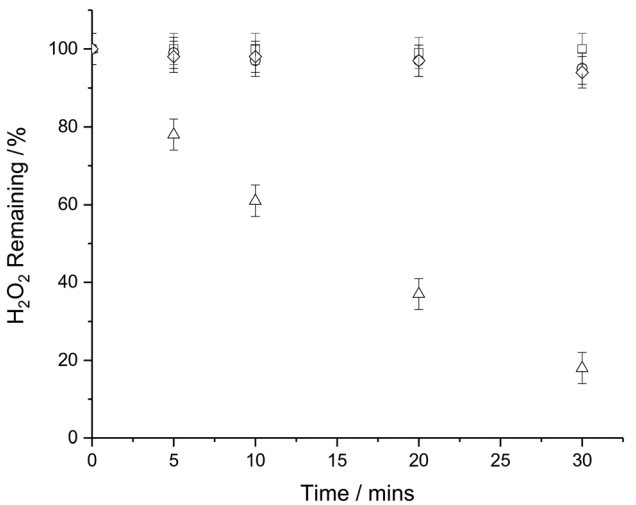

Fig. 5 H_2O_2 decomposition results as a function of time at ambient conditions. Key to symbols: blank (□), TiO_2 only (○), unsupported colloidal AuPd–PVP particles (◊) and TiO_2 supported AuPd particles (△). H_2O_2 decomposition conditions: 4 wt% H_2O_2 in H_2O (10 mL, HPLC grade), in each case 0.66 μmol metal, 9 mg of TiO_2 added under magnetic stirring at ambient temperature and pressure.

higher H_2O_2 decomposition rates in these colloidal systems. Similar tests under ambient conditions using this stabiliser free AuPd nanoparticle solution clearly showed the evolution of bubbles as a result of H_2O_2 decomposition, which could be supressed by the addition of PVP to the reaction mixture. This is in direct contrast to the situation found when using the TiO_2 supported AuPd catalyst, where there seemed to be an interplay between the presence of PVP and the effect of supporting the nanoparticles on inducing H_2O_2 decomposition. The addition of *N*-methyl pyrrolidone as an analogue of the PVP monomer unit was not able to suppress the decomposition in the same way as adding PVP to the stabiliser free colloid, implying that the presence of the hydrophobic alkyl chain backbone could be crucial in controlling the rates of H_2O_2 decomposition in colloidal nanoparticle solutions.

This difference in the H_2O_2 decomposition rates in the absence of pressurised CO_2 could have significant implications in reactions involving aqueous solutions of H_2O_2 as an oxidant or initiator in the absence of acid stabilisers due to the reactivity of support nanoparticles being significantly different to colloidal nanoparticles in terms of H_2O_2 decomposition. Our previous studies on methane oxidation using unsupported and TiO_2 supported colloidal AuPd–PVP nanoparticles have shown that unsupported colloidal catalysts are capable of oxidising methane in the presence of H_2O_2 to produce methanol under mild conditions in which gas phase O_2 incorporation occurred with high efficiency with respect to H_2O_2.[37,40] It was also demonstrated that the TiO_2 supported AuPd colloidal nanoparticles showed low activity in this particular reaction due to high levels of H_2O_2 decomposition.

To extend our previous study and elucidate the role of PVP in this reaction we conducted further methane oxidation experiments with H_2O_2 only as an oxidant using the 1 wt% AuPd/TiO_2 catalyst with extra PVP added to the reaction to identify if this unwanted H_2O_2 decomposition activity, initiated by supporting the AuPd–PVP particles, could be suppressed. Table 2 shows a summary of the catalytic testing results for a colloidal AuPd catalyst prepared with PVP, the TiO_2 supported AuPd–PVP nanoparticles, and the same supported nanoparticles with the addition of extra PVP (giving a metal to PVP ratio 1.2 by weight in the reaction). The results clearly show the superior efficiency of the unsupported AuPd–PVP colloidal system with respect to H_2O_2 efficiency in producing oxygenates. On adding extra PVP to the supported catalyst an improvement was noted with respect to H_2O_2 efficiency and oxygenate production from a H_2O_2: product ratio from 570 to 376, however, the activity of unsupported colloidal system still remained over an order of magnitude better. This demonstrated that the support induced H_2O_2 decomposition could not be fully negated by the addition of further PVP stabiliser.

Further experiments were carried out to investigate if the presence of polymer stabiliser was crucial in achieving the high efficiency of methane oxidation with H_2O_2 and O_2 using colloidal AuPd–PVP nanoparticles. Fig. 6 shows a stark comparison of the catalytic performance of the colloidal metal nanoparticle system synthesised with and without PVP polymer. Without the PVP polymer being present, H_2O_2 consumption during the 30 min reaction period at 50 °C was over 95%, producing minimal oxygenated products. This compares to only 32% H_2O_2 consumption when the colloid incorporated the PVP ligand. The lower H_2O_2 consumption in this latter case resulted in significantly higher oxygenated product formation showing that the polymer is crucial in achieving high reactivity, presumably– by controlling the rate of H_2O_2 decomposition. We then took the stabiliser free colloidal solution prepared in the absence of PVP and added PVP to the methane oxidation reaction. The catalytic performance was significantly improved and indeed, the activity approached that of the colloidal solution prepared with PVP. The H_2O_2 consumption was 48% with significant oxygenate production demonstrating that it is in fact the polymer additive significantly effects the rate of H_2O_2 decomposition on the metal surface and therefore the overall efficiency of methane oxidation. The PVP ligand shell presumably controls the rate of H_2O_2 diffusion to the metal surface and therefore the production of radicals that can interact with the solubilised methane, whose concentration may also be enhanced by the hydrophobic alkyl chains in the organic layer around the metal surface.

In conclusion, we have investigated the role of the PVP ligand shell and TiO_2 support in controlling the reactions of H_2O_2 on AuPd–PVP colloidal particles. These particles display significant activity towards H_2O_2 direct synthesis, hydrogenation and decomposition as well as methane oxidation using H_2O_2 and O_2. We have shown that supporting the PVP stabilised AuPd nanoparticles on TiO_2 increases

Table 2 Summary of methane oxidation reaction results using unsupported AuPd–PVP colloidal nanoparticles, TiO_2 supported AuPd nanoparticles and supported AuPd nanoparticles with additional PVP present (equivalent to metal/PVP ratio of 1.2) using H_2O_2 as the oxidant

	Product amount (μmol)					
Catalyst	CH_3OH	CH_3OOH	HCOOH	CO_2	Oxygenate selectivity/(%)	H_2O_2/products
AuPd–PVP colloid	3.19	9.76	7.04	3.09	86	36
AuPd/TiO_2	0.43	0.00	0.00	1.23	26	575
AuPd/TiO_2 + PVP	0.86	0.43	0.00	1.51	46	326

Reaction conditions; 1000 μmol H_2O_2, reaction temperature = 50 °C, total volume = 10 mL, 30 bar CH_4, reaction time = 30 min, stirring rate = 1500 rpm, 6.6 μmol metal used per reaction.

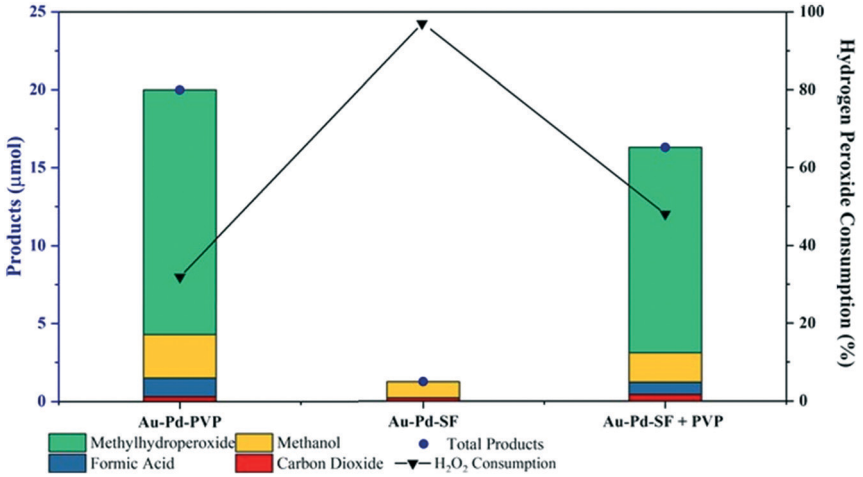

Fig. 6 Comparative methane oxidation tests for AuPd–PVP colloidal nanoparticle sample prepared with PVP (Au–Pd–PVP), stabiliser free (Au–Pd–SF) and stabiliser free with the addition of PVP (Au–Pd–SF + PVP) equivalent to metal/PVP ratio of 1.2. Reaction conditions: pressure (CH_4) = 30 bar, pressure (O_2) = 5 bar, amount of catalyst: 10 mL colloid – 6.6 μmol of metal, 50 μmol H_2O_2, reaction temperature – 50 °C (with a ramp rate of 2.25 °C min^{-1}), stirring rate – 1500 rpm, reaction time – 30 min.

activity towards H_2O_2 decomposition which cannot effectively be suppressed by the addition of extra PVP under our H_2O_2 synthesis or methane oxidation reaction conditions. This could be a result of the formation of more highly faceted alloy particles and an extended metal–support interface – which is absent in the unsupported colloidal AuPd–PVP nanoparticle catalyst. The unsupported particles, when stabilised with PVP, show limited H_2O_2 decomposition activity while being able to produce H_2O_2 at similar rates to supported nanoparticles. However, the use of colloidal particles in extended reactions under flow conditions remains a challenge to translation of this activity to industrial application. Using methane oxidation as a test reaction we demonstrated that this high H_2O_2 decomposition rate is detrimental to the overall efficacy in this case. We also have shown that the colloidal systems require the presence of polymer stabilisers to control the rate of H_2O_2 decomposition. These results clearly demonstrate that for AuPd alloys prepared by colloidal methods, both polymer stabiliser and support effects need to be taken into account when describing the activity of the nanoparticles for a range of reactions involving H_2O_2 such as selective oxidations or reactions that use H_2O_2 or other peroxides as an initiator for oxidation.

Experimental details

Catalyst preparation

Bimetallic Au–Pd nanoparticles were prepared by standard colloidal methods. An aqueous solution of $HAuCl_4$ precursor (Strem Chemicals) and acidic solution of $PdCl_2$ (Sigma Aldrich) precursor (in 0.58 M HCl) were dissolved in 800 mL of de-ionized water (Au : Pd = 1 : 1 by moles) to give a total metal concentration of 0.16 mmol L^{-1}. Polyvinylpyrrolidone (PVP, average molecular weight 1 300 000, Sigma Aldrich) was added as a stabilizer to give the required metal-to-PVP weight ratio (typically 1 : 1.2 (wt/wt)). After 2–3 min of stirring, freshly prepared 0.1 M sodium borohydride ($NaBH_4$, Sigma Aldrich) solution was added such that the molar ratio of $NaBH_4$-to-metal was 5 : 1 (mol/mol). This produced a dark brown colloid which was then left stirring for 30 minutes to ensure that all the metal precursors were reduced to the metallic form. The colloid was concentrated using a roto-evaporator to give a nominal metal loading of 0.66 mmol L^{-1}. The colloid was stored in glass media bottles prior to use. For supported catalysts, the sol prepared as described above was immobilized onto a TiO_2 (P25, Degussa, 1.98 g) or activated carbon (Darco G60) (1.98 g) in the following manner. A sufficient amount of support material was added to ensure a 1 wt% metal loading and the solution was acidified to pH 1 using sulphuric acid to enhance and achieve more homogeneous deposition of nanoparticles. The supernatant solution became clear over a 1 h period after support addition, indicating the deposition process was complete. The sol-immobilized catalyst was then filtered, washed thoroughly with distilled water and then left to dry in an oven at 110 °C for 16 h.

Direct synthesis of H_2O_2

Hydrogen peroxide synthesis was evaluated using a Parr Instruments stainless steel autoclave with a nominal volume of 100 mL and a maximum working pressure of 14 MPa according to our previous optimisation studies.[46] To test each catalyst for H_2O_2 synthesis, the autoclave was charged with catalyst (in each case 0.66 μmol), and solvent (5.6 g MeOH and 2.9 g H_2O). The charged autoclave was then purged three times with 5% H_2/CO_2 (7 bar) before filling with 5% H_2/CO_2 (29 bar), followed by the addition of 25% O_2/CO_2 (11 bar). The temperature was then decreased to 2 °C followed by stirring (1200 rpm) of the reaction mixture for 0.5 h. H_2O_2 productivity was determined by titrating aliquots of the final

solution after reaction with acidified $Ce(SO_4)_2$ (0.01 M) in the presence of ferroin indicator. Duplicate reactions gave H_2O_2 productivities that were typically consistent to ±2% based on multiple titration results.

Degradation of H_2O_2

The autoclave was charged with MeOH (5.6 g), H_2O_2 (50 wt%, 0.69 g), HPLC grade H_2O (2.21 g) and catalyst (0.66 μmol), with the solvent composition equivalent to a 4 wt% H_2O_2 solution. From the solution, 2 aliquots of 0.05 g were removed and titrated with acidified $Ce(SO_4)_2$ solution using ferroin as an indicator to determine an accurate concentration of H_2O_2 at the start of the reaction. The autoclave was pressurised with 5% H_2/CO_2 (29 bar) and cooled to 2 °C. Upon reaching 2 °C the reaction mixture was stirred at 1200 rpm for 0.5 h. After the reaction was complete the catalyst was removed from the reaction solvents and as previously described, *i.e.,* two aliquots (approximately 0.05 g) were titrated against an acidified $Ce(SO_4)_2$ solution using ferroin as an indicator. The degradation activity is reported as the percentage of the initial 4 wt% degraded. Duplicate reactions gave degradation values that were typically consistent to ±1% H_2O_2 decomposed based on multiple titration results.

H_2O_2 degradation conducted in the presence of 5% H_2/CO_2 (29 bar) represents the sum of both hydrogenation and decomposition pathways, while the use of 25% O_2/CO_2 (29 bar) allows for catalytic activity towards H_2O_2 decomposition alone to be determined. All reaction conditions were as described above, apart from the gas atmosphere for the H_2O_2 decomposition studies.

Methane oxidation reaction conditions

Methane oxidation was carried out in a 50 mL glass-lined stainless steel Parr autoclave reactor. The reactor was charged with either colloidal or supported catalyst (0.66 μmol metal per reaction) and H_2O_2 (amount defined in figure captions, Sigma Aldrich, 50 wt% in water). The charged autoclave was sealed and purged three times with methane (10 bar 99.999%, Air Products). It was then pressurized with methane (30 bar) and in some cases oxygen (5 bar, BOC). The mixture was stirred at 1500 rpm and heated to 50 °C at a ramp rate of 2.25 °C min^{-1} and maintained at the reaction temperature for 30 min. At the end of the reaction, the autoclave was cooled in ice to a temperature below 10 °C in order to minimize the loss of volatile products. The reaction gas was removed for analysis in a gas sampling bag.

Product analysis for the methane oxidation reaction

Liquid phase product analysis was carried out using ^{1}H-NMR on a Bruker 500 MHz instrument equipped with a solvent suppression system. Tetramethylsilane (TMS) in $CDCl_3$ was used as an internal standard. The H_2O_2 concentration was determined using a titanium oxalate spectrophotometric method (Agilent, Cary 60). In this procedure, 0.05 to 1.0 mL of reaction sample was acidified using dilute H_2SO_4 before adding potassium titanium oxalate solution (0.5 wt% in water, Sigma Aldrich) to form the yellow pertitanic acid complex with a characteristic absorption peak at 390 nm. Gaseous products were quantified using a Varian 450-GC fitted with a CP-Sil 5CB capillary column (50 m length, 0.32 mm diameter, carrier gas = He), a methaniser unit and both FID and TCD detectors.

Catalyst characterization

TEM. Materials for TEM analysis were prepared by dispersing the colloidal or supported catalyst onto a continuous carbon film supported on a 300-mesh copper TEM grid and allowing the solvent to evaporate. Specimens were examined using the bright-field imaging mode in a JEOL 2000FX transmission electron microscope operating at 200 kV equipped with an Oxford Instruments X-ray energy dispersive (XEDS) spectrometer system.

Explanation of determination of number of surface atoms is reported in the ESI† material. The same approach was used for each catalyst material for comparative purposes assuming spherical particles for colloidal nanoparticles and hemispherical particles for supported nanoparticles.

Conflicts of interest

There are no conflicts to declare.

Acknowledgements

We thank Cardiff University for funding as part of the MaxNet for Chemical Energy Conversion.

References

1 C. J. Jia and F. Schüth, *Phys. Chem. Chem. Phys.*, 2011, **13**, 2457–2487.
2 J. Quinson, S. Neumann, T. Wannmacher, L. Kacenauskaite, M. Inaba, J. Bucher, F. Bizzotto, S. B. Simonsen, L. Theil Kuhn, D. Bujak, A. Zana, M. Arenz and S. Kunz, *Angew. Chem., Int. Ed.*, 2018, **57**, 12338–12341.
3 L. Prati and A. Villa, *Acc. Chem. Res.*, 2014, **47**, 855–863.
4 P. Sonström and M. Bäumer, *Phys. Chem. Chem. Phys.*, 2011, **13**, 19270–19284.
5 S. Maity and M. Eswaramoorthy, *J. Mater. Chem. A*, 2016, **4**, 3233–3237.
6 G. H. Han, S. H. Lee, M. G. Seo and K. Y. Lee, *RSC Adv.*, 2020, **10**, 19952–19960.
7 J. Pritchard, M. Piccinini, R. Tiruvalam, Q. He, N. Dimitratos, J. A. Lopez-Sanchez, D. J. Morgan, A. F. Carley, J. K. Edwards, C. J. Kiely and G. J. Hutchings, *Catal. Sci. Technol.*, 2013, **3**, 308–317.
8 L. F. de L. e Freitas, B. Puértolas, J. Zhang, B. Wang, A. S. Hoffman, S. R. Bare, J. Pérez-Ramírez, J. W. Medlin and E. Nikolla, *ACS Catal.*, 2020, 5202–5207.
9 M. Studer, S. Burkhardt and H. U. Blaser, *Chem. Commun.*, 1999, 1727–1728.

10 H. U. Blaser and M. Studer, *Acc. Chem. Res.*, 2007, **40**, 1348–1356.
11 B. Minder, M. Schürch, T. Mallat, A. Baiker, T. Heinz and A. Pfaltz, *J. Catal.*, 1996, **160**, 261–268.
12 S. Haesuwannakij, T. Kimura, Y. Furutani, K. Okumura, K. Kokubo, T. Sakata, H. Yasuda, Y. Yakiyama and H. Sakurai, *Sci. Rep.*, 2017, **7**, 1–8.
13 L. M. Rossi, J. L. Fiorio, M. A. S. Garcia and C. P. Ferraz, *Dalton Trans.*, 2018, **47**, 5889–5915.
14 J. A. Lopez-Sanchez, N. Dimitratos, C. Hammond, G. L. Brett, L. Kesavan, S. White, P. Miedziak, R. Tiruvalam, R. L. Jenkins, A. F. Carley, D. Knight, C. J. Kiely and G. J. Hutchings, *Nat. Chem.*, 2011, **3**, 551–556.
15 B. Donoeva and P. E. de Jongh, *ChemCatChem*, 2018, **10**, 989–997.
16 G. M. Lari, E. Nowicka, D. J. Morgan, S. A. Kondrat and G. J. Hutchings, *Phys. Chem. Chem. Phys.*, 2015, **17**, 23236–23244.
17 A. Villa, N. Dimitratos, C. E. Chan-Thaw, C. Hammond, L. Prati and G. J. Hutchings, *Acc. Chem. Res.*, 2015, **48**, 1403–1412.
18 J. Xu, H. Zhang, Y. Zhao, B. Yu, S. Chen, Y. Li, L. Hao and Z. Liu, *Green Chem.*, 2013, **15**, 1520–1525.
19 A. Villa, C. Campione and L. Prati, *Catal. Lett.*, 2007, **115**, 133–136.
20 W. C. Ketchie, M. Murayama and R. J. Davis, *J. Catal.*, 2007, **250**, 264–273.
21 L. Abis, N. Dimitritatos, M. Sankar, S. J. Freakley and G. J. Hutchings, *Top. Catal.*, 2019, 1–9.
22 L. Abis, S. J. Freakley, G. Dodekatos, D. J. Morgan, M. Sankar, N. Dimitratos, Q. He, C. J. Kiely and G. J. Hutchings, *ChemCatChem*, 2017, **9**, 2914–2918.
23 S. Kanungo, L. van Haandel, E. J. M. Hensen, J. C. Schouten and M. F. Neira d'Angelo, *J. Catal.*, 2019, **370**, 200–209.
24 S. Kanungo, V. Paunovic, J. C. Schouten and M. F. Neira D'Angelo, *Nano Lett.*, 2017, **17**, 6481–6486.
25 F. Menegazzo, M. Manzoli, M. Signoretto, F. Pinna and G. Strukul, *Catal. Today*, 2015, **248**, 18–27.
26 E. Ghedini, F. Menegazzo, M. Signoretto, M. Manzoli, F. Pinna and G. Strukul, *J. Catal.*, 2010, **273**, 266–273.
27 N. M. Wilson, P. Priyadarshini, S. Kunz and D. W. Flaherty, *J. Catal.*, 2018, **357**, 163–175.
28 J. Pritchard, L. Kesavan, M. Piccinini, Q. He, R. Tiruvalam, N. Dimitratos, J. A. Lopez-Sanchez, A. F. Carley, J. K. Edwards, C. J. Kiely and G. J. Hutchings, *Langmuir*, 2010, **26**, 16568–16577.
29 G. M. Lari, B. Puértolas, M. Shahrokhi, N. López and J. Pérez-Ramírez, *Angew. Chem.*, 2017, **129**, 1801–1805.
30 S. J. Freakley, Q. He, J. H. Harrhy, L. Lu, D. A. Crole, D. J. Morgan, E. N. Ntainjua, J. K. Edwards, A. F. Carley, A. Y. Borisevich, C. J. Kiely and G. J. Hutchings, *Science*, 2016, **351**, 965–968.
31 J. K. Edwards, B. Solsona, E. Ntainjua, N. A. F. Carley, A. A. Herzing, C. J. Kiely and G. J. Hutchings, *Science*, 2009, **323**, 1037–1041.
32 P. Beltrame, M. Comotti, C. Della Pina and M. Rossi, *Appl. Catal., A*, 2006, **297**, 1–7.
33 J. Zhao, W. Y. Hernández, W. Zhou, Y. Yang, E. I. Vovk, M. Capron and V. Ordomsky, *ChemCatChem*, 2020, **12**, 238–247.
34 A. García-Trenco, E. R. White, A. Regoutz, D. J. Payne, M. S. P. Shaffer and C. K. Williams, *ACS Catal.*, 2017, **7**, 1186–1196.
35 Y. Nomura, T. Ishihara, Y. Hata, K. Kitawaki, K. Kaneko and H. Matsumoto, *ChemSusChem*, 2008, **1**, 619–621.
36 T. Deguchi, H. Yamano, S. Takenouchi and M. Iwamoto, *Catal. Sci. Technol.*, 2018, **8**, 1002–1015.
37 N. Agarwal, S. J. Freakley, R. U. McVicker, S. M. Althahban, N. Dimitratos, Q. He, D. J. Morgan, R. L. Jenkins, D. J. Willock, S. H. Taylor, C. J. Kiely and G. J. Hutchings, *Science*, 2017, **358**, 223–227.
38 G. Giorgianni, S. Abate, G. Centi and S. Perathoner, *ChemCatChem*, 2019, **11**, 550–559.
39 J. Radnik, C. Mohr and P. Claus, *Phys. Chem. Chem. Phys.*, 2003, **5**, 172–177.
40 R. McVicker, N. Agarwal, S. J. Freakley, Q. He, S. Althahban, S. H. Taylor, C. J. Kiely and G. J. Hutchings, *Catal. Today*, 2020, **342**, 32–38.
41 T. Ishihara, R. Nakashima, Y. Ooishi, H. Hagiwara, M. Matsuka and S. Ida, *Catal. Today*, 2015, **248**, 35–39.
42 J. K. Edwards, B. E. Solsona, P. Landon, A. F. Carley, A. Herzing, C. J. Kiely and G. J. Hutchings, *J. Catal.*, 2005, **236**, 69–79.
43 Y. F. Han and J. H. Lunsford, *J. Catal.*, 2005, **230**, 313–316.
44 R. C. Tiruvalam, J. C. Pritchard, N. Dimitratos, J. A. Lopez-Sanchez, J. K. Edwards, A. F. Carley, G. J. Hutchings and C. J. Kiely, *Faraday Discuss.*, 2011, **152**, 63–86.
45 C. Deraedt, L. Salmon, S. Gatard, R. Ciganda, R. Hernandez, J. Ruiz and D. Astruc, *Chem. Commun.*, 2014, **50**, 14194–14196.
46 M. Piccinini, E. Ntainjua, N. J. K. Edwards, A. F. Carley, J. A. Moulijn and G. J. Hutchings, *Phys. Chem. Chem. Phys.*, 2010, **12**, 2488–2492.